Heart and Vessels
https://doi.org/10.1007/s00380-018-1180-y

ORIGINAL ARTICLE

The seamless integration of three-dimensional rotational angiography images into electroanatomical mapping systems to guide catheter ablation of atrial fibrillation

Satoshi Fujita[1] · Eitaro Fujii[1] · Yoshihiko Kagawa[1] · Katsuhiro Inoue[2] · Tsuyoshi Yamada[2] · Masaaki Ito[1]

Received: 7 December 2017 / Accepted: 27 April 2018

Abstract
It is important to visually confirm radiofrequency ablation lesions during atrial fibrillation (AF) ablation for procedural efficiency, which requires the integration of a three-dimensional (3D) left atrial image reconstructed from computed tomography (CT) or a magnetic resonance imaging. However, an EP Navigator allows seamless integration of 3D anatomy obtained through 3D rotational angiography (3D-ATG) into an electroanatomical mapping system. We hypothesized that 3D-ATG can be used during AF ablation while significantly reducing the effective dose (ED) and without compromising image morphology compared to a 3D-CT image. Organ dose was measured at 37 points with a radiophotoluminescence glass dosimeter inserted in an anthropomorphic Rando Phantom. The ED was calculated by multiplying the organ dose by the tissue weighting factor. The dose-area product (DAP)-to-ED conversion factor was calculated by measuring the DAP during radiation exposure. The ED for the CT examination was estimated from the dose-length product with a conversion factor of 0.014. ED was calculated from DAP measurements in 114 patients undergoing AF ablation using 3D-ATG. The DAP-to-ED conversion factor for 3D-ATG was 2.4×10^{-4} mSv/mGy cm^2 in our hospital. The mean DAP for all patients was 7777 ± 1488 mGy cm^2 for the 3D-ATG of the left atrium. The corresponding ED for 3D-ATG was 1.9 ± 0.4 mSv. The ED for CT examinations was 13.6 ± 4.2 mSv ($P<0.001$). 3D-ATG can be used during AF ablation while significantly reducing the ED and without compromising image morphology.

Keywords Atrial fibrillation · Catheter ablation · Rotational angiography · Seamless integration of 3D anatomy · Effective dose

Introduction

Catheter ablation of drug-resistant paroxysmal and persistent atrial fibrillation (AF) is becoming a reasonable alternative therapy in symptomatic patients. When treating patients undergoing catheter ablation for AF, it is essential to visualize the three-dimensional (3D) structure of the left atrium (LA) [1–4]. We can use CARTO® or EnSite/NavX® as a 3D mapping system; however, both need integration of a 3D LA image reconstructed from a computed tomography (CT) image, a magnetic resonance imaging (MRI), or intracardiac echocardiography. These processes are time consuming and are associated with a high radiation exposure for CT scanning.

However, 3D rotational angiography of LA (3D-ATG) represents a method of creating CT-like 3D images. EP Navigator system visualizes 3D LA and pulmonary vein (PV) anatomy and the position of the ablation catheter in real time. This information is combined with live fluoroscopy data to show the exact position of catheters in relation to the detailed 3D anatomy of the heart during AF ablation. Prior studies have demonstrated that the diagnostic value of 3D-ATG is comparable to that of CT imaging [5–7]. The EP Navigator system provides several functions, such as 3D-ATG, automatic segmentation, creation of surface renderings of the heart, exports to mapping, endo views, and point tagging [8]. Moreover, the EP Navigator now supports

✉ Eitaro Fujii
fujii-e@clin.medic.mie-u.ac.jp

[1] Department of Cardiology and Nephrology, Mie University Graduate School of Medicine, 2-174 Edobashi, Tsu, Mie 514-8507, Japan

[2] Department of Radiological Technology, Mie University Hospital, 2-174 Edobashi, Tsu, Mie 514-8507, Japan

Published online: 07 May 2018

the seamless integration of the 3D anatomy obtained through 3D-ATG into the CARTO® 3 system (Fig. 1). We assessed the hypothesis that AF ablation using 3D-ATG would be feasible with a significant reduction in the effective dose (ED) and without compromising image morphology compared to a 3D-CT image. The anatomical accuracy of 3D LA-PV images produced by 3D-ATG and 3D-CT was also compared.

Methods

Study population

The study included one hundred and fourteen consecutive patients who underwent catheter ablation for AF in our hospital between May 2015 and April 2016. Informed written consent was obtained from each patient prior to the procedure. This was an observational study, 33 patients could not have a CT scanning before ablation as following reasons; 8 patients underwent CT scanning at 1st or 2nd session of AF ablation, 4 patients received CT scanning to evaluate another disease before ablation, 8 patients could not make a reservation for CT examination before admission, 6 patients had a renal insufficiency (serum creatinine level > 1.5 mg/dL), 4 patients had an overt heart failure, 2 patients had asthma, and 1 patient had a history of contrast medium allergies. Eighty-one patients underwent pre-procedural CT with reconstruction of the LA, PV and esophagus within 4 weeks of their admission. All patients also underwent pre-procedural transesophageal echocardiography to exclude left atrial thrombus. This study was approved by the Mie University Hospital Institutional Review Boards (Reference number: 3038) and all patients gave their informed consent.

Organ dose and surface radiation dose measurement

An adult female anthropomorphic phantom (Rando phantom, Kyoto Kagaku Co., LTD, Kyoto, Japan) was used to simulate an adult patient [9]. The phantom contains bone, lungs, thyroids, breasts, esophagus and other organs, with compositions based on previously published data, and using tissue substitutes for radiation dosimetry. Thirty-seven high-sensitivity metal oxide semiconductor field-effect transistor (MOSFET) dosimeters (Dose Ace GD-352, Asahi Techno Glass, Tokyo, Japan) were placed in selected organs and tissue types in the phantom (Fig. 2). Most MOSFETs were placed in the trunk of the body, and each organ dose was measured by a calibrated 6-cm^3 ion chamber at the beam qualities of the imaging protocols being investigated. The ED was calculated by multiplying the organ dose by the tissue weighting factor [10]. The dose-area product (DAP)-to-ED conversion factor was calculated by measuring the DAP at the time of radiation exposure.

Surface radiation dose was measured using the Gafchromic Films in the phantom from 16 skin areas. Radiochromatic film (Gafchromic® XRQA2, International Speciality Products, New Jersey, NJ, USA) was used to determine the proportion of beam on/off time during one 360° rotation. The film was wrapped around the exit port of the scanner gantry and scanned using the prospectively gated cardiac protocol.

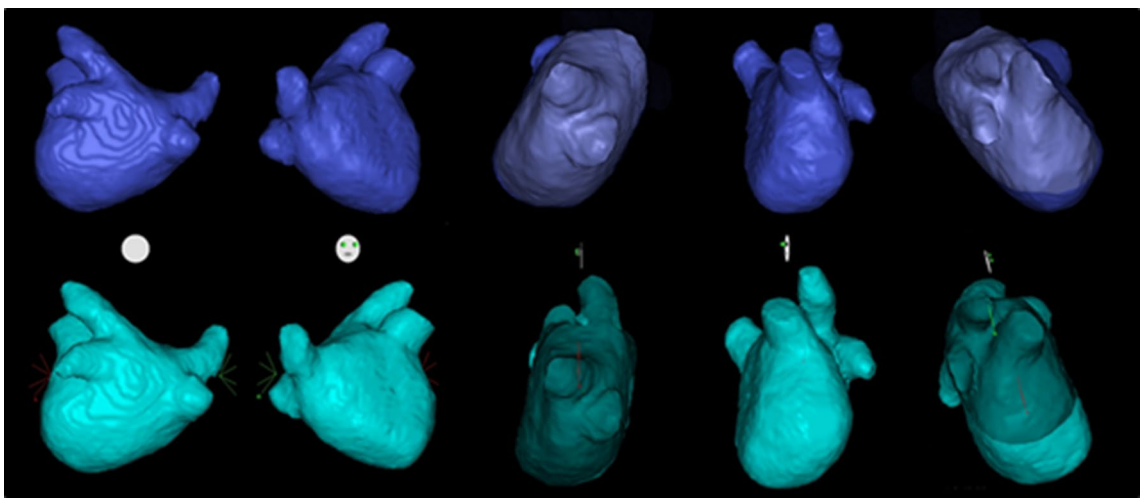

Fig. 1 Outer and inner view of the LA and PVs. Upper panels show the surface rendering of the left atrium (LA) and pulmonary veins (PVs) created from rotational angiography. Lower panels represent the 3D images of LA and PVs reconstructed by CARTO® 3 using the integrated surface rendering from the EP Navigator in the same patients

Fig. 2 Anthropomorphic phantom. Left panel shows the Rand Phantom. Right upper panel shows a radiophotoluminescence glass dosimeter. The glass dosimeters are inserted in the 37 position of an anthropomorphic Rando Phantom (Right lower panel)

Pre-procedural cardiac multi-detector computed tomography

Patients underwent pre-procedural contrast-enhanced Chest CT using a 96 multislice CT scanner (SOMATOM FORCE, Siemens Healthcare, Forchheim, Germany) with the following scan parameters: 120 kV tube voltage, 160 mAs tube current time-product, 96 × 192 mm detector size, and 0.5 s rotation time. Patients underwent reconstruction of the LA, PV and esophagus within 4 weeks of admission. The CT scan was performed during an end-expiratory breath-hold phase and following the injection of 100 mL of an iodinated contrast medium. The reconstruction of 3D-images was performed with a slice of 0.6 mm thickness [11]. Atrial end-diastolic imaging data were recorded and used for 3D cardiac reconstruction on a 512–512-pixel matrix with the use of the EP Navigator workstation (Phillips Medical Systems, Best, The Netherlands).

Intra-procedural three-dimensional rotational angiography of LA and PVs

All imaging was performed using a biplane flat-panel detector angiographic suite (Allura Xper FD10/10 angio system; Philips Healthcare, Best, Netherlands). Intraoperative 3D-ATG was performed with 15 mL of contrast medium + 15 mL of saline injected by hand directly into the bilateral upper pulmonary veins via the Swartz long sheaths placed in the left and right superior pulmonary veins during rapid ventricular pacing at 200 beats per minute. 3D-ATG was performed from the right oblique at 59° to the left oblique at 100° of C-arm rotation at a sampling rate of 30 frames per second for a total of 3.8 s [5, 12].

EP navigator and fluoroscopy registration

After the rotational angiography, the data were automatically transported from the FD10/10 detector System to the EP

Navigator Workstation. The 3D LA-PV images were reconstructed using the standard 3D reconstruction algorithms available on the EP Navigator Workstation within 1 min, and were seamlessly integrated into the CARTO® 3 system using the local area network in our hospital within 2–3 min. The 3D LA-PV image was integrated with the live fluoroscopy.

Quantitative evaluation of PVs and LA

The PV ostia from the CT and 3D-ATG reconstruction images were measured by two independent cardiologists using the same software (EP Navigator 2.2, Philips Inc.) [6]. The diameter of the four PV ostia were measured using the image of the coronal plane. The LA was measured at three different sites. Longitudinal diameter was defined as the distance between the LA roof and bottom. Lateral diameter was defined as the distance between the upper PVs, and the occipito-frontal diameter was defined as the distance from the LA anterior wall to the posterior wall facing the thoracic spine at the level of the left carina of the PVs (Fig. 3).

Radiation exposure of CT and 3D-ATG

The ED of CT was calculated using the CT-generated dose-length product (DLP) and a standard conversion factor of 0.014 mSv/mGy cm [13]. The ED of 3D-ATG was calculated using the DAP during the ablation procedure, and the DAP-to-ED conversion factor at our facility was estimated by an anthropomorphic phantom model.

Statistical analysis

Patient characteristics and the clinical outcome of both groups were described using descriptive statistics. Continuous variables are expressed as a mean ± standard deviation (SD) and categorical variables as absolute values and percentages. Results were analyzed using the SPSS 22.0 software (SPSS Inc., Chicago, IL, USA) and rendered as a mean ± standard deviation (SD) of the difference in measurements between CT and 3D-ATG. Categorical data were analyzed using a chi-squared test or a Fisher's exact test. Continuous data were evaluated using unpaired Student's *t* test or nonparametric Mann–Whitney when dealing with non-normal distribution. The diameter of LA and the four PV ostia in CT and 3D-ATG image were analyzed based on the calculation of correlation coefficients. A P value <0.05 was considered statistically significant.

Results

Patient characteristics

Patient characteristics are summarized in Table 1. Body mass index was around 24 kg/m^2. Most patients had paroxysmal AF and preserved left ventricular function. The mean LA diameter was 40 ± 6 mm. The mean $CHADS_2$ and CHA_2DS_2-VASc scores were 1 ± 1 and 2 ± 2 points, respectively.

Organ dose and effective dose

The actual measured value from each dosimeter and the calculated effective dose of each organ are listed in Table 2. The ED was 0.787 mSv and the DAP was 3279 mGy cm^2. The DAP-to-ED conversion coefficient was 2.4×10^{-4} mSv/mGy cm^2, estimated using the phantom models in our facility.

Surface radiation dosage

Gafchromic film dosimetry measurements comparing two imaging techniques in the same phantom were obtained (Table 3). Surface radiation dose in 3D-ATG was significantly lower than that in CT ($P < 0.001$).

Comparison of effective dose between 3D-ATG and 3D-CT

The DAP was 7777 ± 1488 mGy cm^2 and the estimated ED was 1.9 ± 0.4 mSv during 3D-ATG in the 81 study patients. The DLP and the estimated ED during plain, early phase contrast-enhanced scanning and delayed phase contrast-enhanced CT scanning was 962 ± 324, 386 ± 125, 170 ± 75 mGy cm, and 5.4 ± 1.8, 5.3 ± 1.9, 2.4 ± 0.9 mSv, respectively (Table 4). The ED of 3D–ATG was significantly lower than that of CT in each scanning method.

Quantitative evaluation of PVs and LA

Table 5 shows the parameter of the mean diameter of the four PV ostia, and LA longitudinal diameter, LA lateral diameter and LA occipito-frontal diameter obtained by 3D-CT and 3D-ATG. All methods showed close correlation for every PV. The correlation coefficients for LA longitudinal, lateral, occipito-frontal diameter were 0.798, 0.760 and 0.726, respectively.

Discussion

The ED of 3D-ATG was significantly lower than those from the CT scan, especially surface radiation dosage. Moreover, 3D-ATG was an intra-procedural imaging modality that

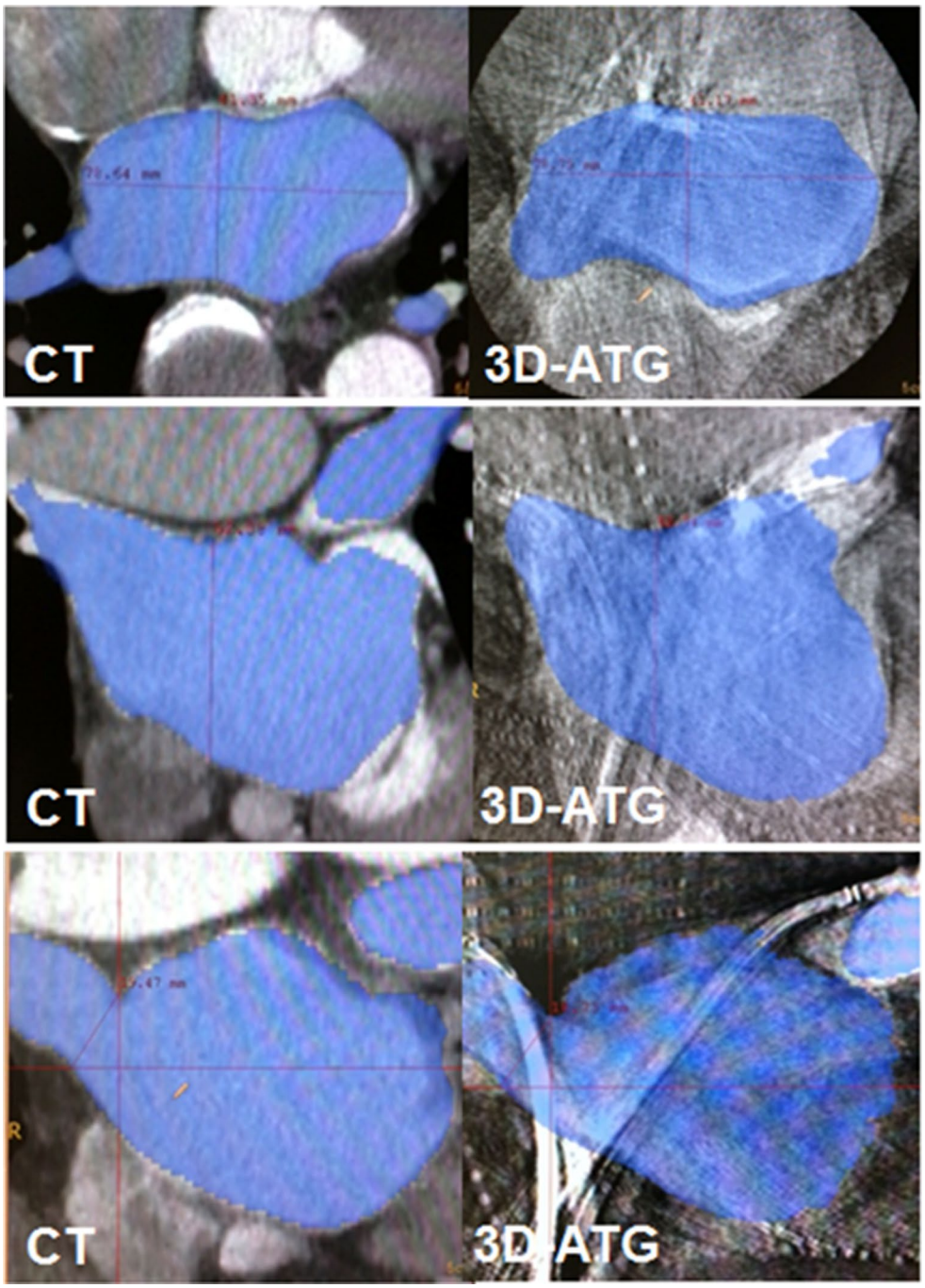

Fig. 3 Measurement of the LA and PV diameters. Upper panels show measurement of left atrial (LA) occipito-frontal diameter and LA lateral diameter using transverse plane on a parallelized cutting level between computed tomography (CT) and 3-dimensional rotational angiography (3D-ATG). Middle panels show measurement of LA longitudinal diameter using coronal plane on a parallelized cutting level between CT and 3D-ATG. Lower panels show measurement of pulmonary vein ostial diameter using coronal plane on a parallelized cutting level between CT and 3D-ATG

provided a level of anatomical accuracy comparable to that of CT.

The estimation of organ and effective doses was performed using Monte Carlo simulations of photon interactions within a simplified mathematical model of the human body [14–17]. However, calculated dose values should be verified through dose measurements using physical phantoms with the same exposure conditions as the calculation. In this study, we performed direct measurements of absorbed doses at various organ and tissue positions in the

Table 1 Patients' characteristics

Study population ($n=114$)	Value
Age, years	65 ± 11
Gender (male), *n* (%)	79 (69)
Body mass index, kg/m^2	24 ± 4
Paroxysmal AF/persistent AF, *n*	82/32
First session/2nd or 3rd session, *n*	89/25
Atrial Flutter, *n*	34
LA diameter, mm	40 ± 6
LV ejection fraction, %	65 ± 10
$CHADS_2$ score	1 ± 1
CHA_2DS_2-VASc score	2 ± 2

AF atrial fibrillation, *LA* left atrium, *LV* left ventricle

Table 2 Organ and effective dose for exposures involved in 3D-ATG

Organ	Total organ dose (μGy)	Effective dose (mSv)
Gonad	12	0.000
Bone marrow	1009	0.190
Colon	246	0.004
Lung	9185	0.212
Stomach	656	0.061
Bladder	10	0.000
Liver	1555	0.024
Esophagus	1952	0.030
Thyroid gland	82	0.003
Skin	9714	0.003
Bone surface	13,006	0.000
Breast	2739	0.036
Other	649	0.036

3D-ATG three-dimensional rotational angiography

Table 3 Surface radiation dose in CT and 3D-ATG estimated using the phantom models

Gafchromic film portion		Surface radiation dosage (mGy)	
		CT	3D-ATG
1	Axilla (right superior)	1.09	0.060
2	Chest (right superior)	1.21	0.017
3	Chest (mid superior)	1.35	0.059
4	Chest (left superior)	0.87	0.030
5	Axilla (left superior)	0.80	0.076
6	Axilla (right inferior)	0.86	0.044
7	Chest (right inferior)	1.17	0.022
8	Chest (mid inferior)	1.15	0.025
9	Chest (left inferior)	0.95	0.042
10	Axilla (left inferior)	0.83	0.068
11	Dorsal (left superior)	0.86	0.038
12	Dorsal (mid superior)	1.35	0.015
13	Dorsal (right superior)	1.14	0.001
14	Dorsal (left inferior)	0.73	0.039
15	Dorsal (mid inferior)	1.14	0.055
16	Dorsal (right inferior)	0.77	0.053
Average		1.02 ± 0.21	0.040 ± 0.021*

3D-ATG three-dimensional rotational angiography, *CT* computed tomography

*$P < 0.001$ vs CT

Table 4 Comparison of effective dose between the 3D-ATG and CT imaging

Radiation dose	3D-ATG	CT		
		Plain	Enhanced (early phase)	Enhanced (delayed phase)
DAP (mGy cm^2)	7777 ± 1488			
DLP (mGy cm)		962 ± 324	386 ± 125	170 ± 750
ED (mSv)	1.9 ± 0.4	5.4 ± 1.8*	5.3 ± 1.9*	2.4 ± 0.9*

3D-ATG three-dimensional rotational angiography, *CT* computed tomography, *DAP* dose-area product, *DLP* dose-length product, *ED* effective dose

*$P < 0.001$ vs 3D-ATG

anthropomorphic phantoms. It would be significant to evaluate organ and the effective doses to patients during procedures in our laboratory, as the DAP-to-ED conversion factor may vary from institution to institution.

To the best of our knowledge, there are several research data available that assess the radiation exposure of AF ablation guided by 3D-ATG vs. 3D-CT. Tang et al. compared radiation exposure of catheter ablation for AF between 3D-CT scans and 3D-ATG of LA and PVs [6]. They prospectively assigned 46 patients referred to their institution for catheter ablation of AF. The radiation exposure in 3D-ATG was significantly less than that in CT scanning (2.7 ± 0.9 vs. 24.9 ± 3.1 mSv, $P < 0.001$). However, they used Monte Carlo simulations to estimate the ED during 3D-ATG. Anond et al. performed randomized prospective study comparing the ED guided by 3D-ATG vs. 3D-CT [18]. In this study, the ED during 3D-ATG and 3D-CT was 3.0 ± 0.9 and 9.3 ± 4.4 mSv, respectively. Same study by Kriatselis et al. reported that the radiation exposure in 3D-ATG was substantially less than that in 3D-CT (2.2 ± 0.2 vs. 20.4 ± 7.4 mSv, $P < 0.05$) [19]. Li JH, et al. evaluated the feasibility and accuracy of intra-procedural 3D-ATG. They demonstrated that the radiation exposure with 3D-ATG was significantly reduced compared with preprocedural 3D-CT (2.1 ± 0.3 vs. 13.8 ± 2.4 mSv) [20]. In these studies, the DAP-to-ED conversion factor at their facility was not

Table 5 Comparable evaluation between the CT and 3D-ATG image

	CT	3D-ATG	*r*	*P* value
RSPV (mm)	20 ± 3	20 ± 3	0.496	< 0.05
RIPV (mm)	17 ± 3	189 ± 4	0.781	< 0.001
LSPV (mm)	21 ± 4	20 ± 3	0.745	< 0.001
LIPV (mm)	16 ± 4	15 ± 4	0.866	< 0.001
LA longi (mm)	66 ± 7	66 ± 5	0.798	< 0.001
LA occipito (mm)	40 ± 7	37 ± 7	0.726	< 0.01
LA lateral (mm)	74 ± 8	74 ± 8	0.760	< 0.001

3D-ATG three-dimensional rotational angiography, *CT* computed tomography, *LA* left atrium, *LA lateral* LA lateral diameter, *LA longi* LA longitudinal diameter, *LA occipito* LA occipito-frontal diameter, *LIPV* left inferior pulmonary vein, *LSPV* left superior pulmonary vein, *RIPV* right inferior pulmonary vein, *RSPV* right superior pulmonary vein

estimated using an anthropomorphic phantom model. The ED during fluoroscopy or cine-angiography varies in each institution or in each cine-angio machine and imaging angle when this type of simulation is used. Thus, we calculated DAP-to-ED conversion coefficient using the anthropomorphic phantom in our laboratory.

Biologic effects resulting from radiation exposure are classified into stochastic effects and deterministic effects based on the difference between the dose–response relationships. Skin injuries can occur in catheter ablation, percutaneous coronary intervention, and other procedures that can involve the delivery of large amounts of radiation [21]. Threshold doses exist for deterministic effects, such as skin and lens injuries. The threshold skin entrance dose for skin injury of early transient erythema is 2 Gy, which is the earliest change after acute delivery of radiation. In this study, the radiation dose during either the 3D-ATG or CT was below the threshold dose, meaning skin injury would not occur.

The ED serves as an index of the risk for carcinogenesis and genetic effects resulting from low-dose exposure in individual persons [22]. The probability of the onset of cancer due to radiation probably rises in proportion to the increase in dose, without a threshold value [23]. The ED of 3D-ATG was significantly lower than those of the CT scan in this study.

Limitations

There were some limitations in our study. First, radiation reduction techniques, such as tube voltage adjustment, dose pulsing, ECG gating, or the use of a dual-source CT system, were not systematically performed. However, the ED during CT examination was very low in this study: 5.3 ± 1.9 mSv for early phase and 2.4 ± 0.9 mSv for delayed phase contrast enhancement. Hur et al. reported that dual-enhanced single-scan CT with prospective electrocardiographic gating was a noninvasive and sensitive modality for detecting left atrial appendage thrombus and had an acceptable radiation dose of 3.1 mSv. They used a second-generation dual-source CT scanner (Somatom Definition Flash; Siemens Medical Solutions, Erlangen, Germany) and scanning was performed with the second injection of contrast agent, 180 s after injection of the first bolus of contrast agent [24]. Our results of radiation exposure during CT were not high compared with the report from Hur et al. Second, with the CT image, it is possible to assess the state of the tissue surrounding the heart, the presence of abnormal vein draining to the left atrium, the shape of the left atrial appendage, and the presence or absence of left atrial thrombus before ablation procedure; however, the patients receive additional high radiation exposure. Finally, the study was not designed to assess the impact of 3D-ATG or 3D-CT integration on procedural outcomes or safety aspects, though several studies demonstrated the utility and feasibility of catheter ablation for atrial fibrillation using 3D-ATG.

Conclusion

AF ablation using 3D-ATG is possible with a significant reduction in the ED and without compromising image morphology.

Compliance with ethical standards

Conflict of interest Masaaki Ito received honorarium equal to or more than 500,000 yen from Daiichi Sankyo Co., Ltd., Bayer Holding Ltd., and Takeda Pharmaceutical Co., Ltd. in 2017. The Department of Cardiology and Nephrology, Mie University Graduate School of Medicine is supported in part by unrestricted research grants of equal to or more than 1,000,000 yen from Bristol-Myers Squibb K.K., MSD K.K., Shionogi & Co., Ltd., Otsuka Pharma Inc. and Takeda Pharmaceutical Co., Ltd. in 2017. The other authors declare that they have no conflict of interest.

References

1. Mikaelian BJ, Malchano ZJ, Neuzil P, Weichet J, Doshi SK, Ruskin JN, Reddy VY (2005) Images in cardiovascular medicine. Integration of 3-dimensional cardiac computed tomography images with real-time electroanatomic mapping to guide catheter ablation of atrial fibrillation. Circulation 112:e35–e36
2. Noseworthy PA, Malchano ZJ, Ahmed J, Holmvang G, Ruskin JN, Reddy VY (2005) The impact of respiration on left atrial and pulmonary venous anatomy: implications for image-guided intervention. Heart Rhythm 2:1173–1178
3. Dong J, Calkins H, Solomon SB, Lai S, Dalal D, Lardo AC, Brem E, Preiss A, Berger RD, Halperin H, Dickfeld T (2006) Integrated electroanatomic mapping with three-dimensional computed tomographic images for real-time guided ablations. Circulation 113:186–194

4. Kistler PM, Earley MJ, Harris S, Abrams D, Ellis S, Sporton SC, Schilling RJ (2006) Validation of three-dimensional cardiac image integration: use of integrated CT image into electroanatomic mapping system to perform catheter ablation of atrial fibrillation. J Cardiovasc Electrophysiol 17:341–348
5. Li JH, Haim M, Movassaghi B, Mendel JB, Chaudhry GM, Haffajee CI, Orlov MV (2009) Segmentation and registration of three-dimensional rotational angiogram on live fluoroscopy to guide atrial fibrillation ablation: a new online imaging tool. Heart Rhythm 6:231–237
6. Tang M, Kriatselis C, Ye G, Nedios S, Roser M, Solowjowa N, Fleck E, Gerds-Li JH (2009) Reconstructing and registering three-dimensional rotational angiogram of left atrium during ablation of atrial fibrillation. Pacing Clin Electrophysiol 32:1407–1416
7. Kriatselis C, Nedios S, Akrivakis S, Tang M, Roser M, Gerds-Li JH, Fleck E, Orlov M (2011) Intraprocedural imaging of left atrium and pulmonary veins: a comparison study between rotational angiography and cardiac computed tomography. Pacing Clin Electrophysiol 34:315–322
8. Knecht S, Skali H, O'Neill MD, Wright M, Matsuo S, Chaudhry GM, Haffajee CI, Nault I, Gijsbers GH, Sacher F, Laurent F, Montaudon M, Corneloup O, Hocini M, Haïssaguerre M, Orlov MV, Jaïs P (2008) Computed tomography-fluoroscopy overlay evaluation during catheter ablation of left atrial arrhythmia. Europace 10:931–938
9. Hurwitz LM, Yoshizumi TT, Goodman PC, Frush DP, Nguyen G, Toncheva G, Lowry C (2007) Effective dose determination using an anthropomorphic phantom and metal oxide semiconductor field effect transistor technology for clinical adult body multidetector array computed tomography protocols. J Comput Assist Tomog 31:544–549
10. [No authors listed] (2007) The 2007 Recommendations of the international commission on radiological protection ICRP publication 103. Ann ICRP 37:1–332
11. Ejima K, Shoda M, Yagishita D, Futagawa K, Yashiro B, Sato T, Manaka T, Nakajima T, Ohmori H, Hagiwara N (2010) Image integration of three-dimensional cone-beam computed tomography angiogram into electroanatomical mapping system to guide catheter ablation of atrial fibrillation. Europace 12:45–51
12. Nölker G, Gutleben KJ, Asbach S, Vogt J, Heintze J, Brachmann J, Horstkotte D, Sinha AM (2011) Intracardiac echocardiography for registration of rotational angiography-based left atrial reconstructions: a novel approach integrating two intraprocedural three-dimensional imaging techniques in atrial fibrillation ablation. Europace 13:492–498
13. Tan SK, Yeong CH, Ng KH, Abdul Aziz YF, Sun Z (2016) Recent update on radiation dose assessment for the state-of-the-art coronary computed tomography angiography protocols. PLoS One 11:e0161543
14. Vano E, Gonzalez L, Ten JL, Fernandez JM, Guibelalde E, Macaya C (2001) Skin dose and dose-area product values for interventional cardiology procedures. Br J Radiol 74:48–55
15. Delichas MG, Psarrakos K, Molyvda-Athanassopoulou E, Giannoglou G, Hatziioannou K, Papanastassiou E (2003) Radiation doses to patients undergoing coronary angiography and percutaneous transluminal coronary angioplasty. Radiat Prot Dosim 103:149–154
16. Stisova V (2004) Effective dose to patient during cardiac interventional procedures (prague workplaces). Radiat Prot Dosim 111:271–274
17. Bor D, Sancak T, Olgar T, Elcim Y, Adanali A, Sanlidilek U, Akyar S (2004) Comparison of effective doses obtained from dose-area product and air kerma measurements in interventional radiology. Br J Radiol 77:315–322
18. Anand Rishi, Gorev Maxim V, Poghosyan Hermine, Pothier Lindsay, Matkins John, Kotler Gregory, Moroz Sarah, Armstrong James, Nemtsov Sergei V, Orlov Michael V (2016) Prospective randomized comparison of rotational angiography with three-dimensional reconstruction and computed tomography merged with electro-anatomical mapping: a two center atrial fibrillation ablation study. J Interv Card Electrophysiol 46:71–79
19. Kriatselis C, Nedios S, Akrivakis S, Tang M, Roser M, Gerds-Li JH, Fleck E, Orlov M (2011) Intraprocedural imaging of left atrium and pulmonary veins: a comparison study between rotational angiography and cardiac computed tomography. Pacing Clin Electrophysiol 34:315–322
20. Li JH, Haim M, Movassaghi B, Mendel JB, Chaudhry GM, Haffajee CI, Orlov MV (2009) Segmentation and registration of three-dimensional rotational angiogram on live fluoroscopy to guide atrial fibrillation ablation: a new online imaging tool. Heart Rhythm 6:231–237
21. Nahass GT (1995) Fluoroscopy and the skin: implications for radiofrequency catheter ablation. Am J Cardiol 76:174–176
22. Perisinakis K, Damilakis J, Theocharopoulos N, Manios E, Vardas P, Gourtsoyiannis N (2001) Accurate assessment of patient effective radiation dose and associated detriment risk from radiofrequency catheter ablation procedures. Circulation 104:58–62
23. JCS Joint Working Group (2010) Guideline for radiation safety in interventional cardiology (JCS 2011)—digest version. Circ J 74:2760–2785
24. Hur Jin, Kim YJ, Lee HJ, Nam JE, Ha JW, Heo JH, Chang HJ, Kim HS, Hong YJ, Kim HY, Choe KO, Choi BW (2011) Dual-enhanced cardiac CT for detection of left atrial appendage thrombus in patients with stroke. A prospective comparison study with transesophageal echocardiography. Stroke 42:2471–2477